Available online at www.sciencedirect.com
SCIENCE DIRECT
Journal of Power Sources 155 (2006) 182–189
JOURNAL OF POWER SOURCES
www.elsevier.com/locate/jpowsour

Study of fuel cell structure and heating method Development of JARI's standard single cell

Yoshiyuki Hashimasa*, Tomoaki Numata, Kenzo Moriya, Shogo Watanabe

FC-EV Center Hydrogen and Fuel Cell Performance Research, Japan Automobile Research Institute, Japan

Received 30 November 2004; accepted 15 February 2005
Available online 1 June 2005

Abstract

The effects of cell configuration, materials, assembly method, and temperature control method on the performance of Japan Automobile Research Institute's (JARI's) standard single cell were investigated in order to reproducibly estimate the influence of impurities. From the results, active electrode area, flow channel configuration, clamping torque, and thermal design of the cell were optimized. JARI's standard single cells are used for investigating hydrogen fuel, because they are easily assembled and disassembled, have uniform electric generation performance from one unit to another, and have high reproducibility from one test to another.

Keywords: Hydrogen fuel; Cell configuration; Cell materials; Cell assembly method; Temperature control method; JARI's standard single cell

1. Introduction

Practical fuel cell stacks need a large electrode area and many cells for automobile use. Single cells, characterized by their compact size, are used in many ways including for the evaluation of electrode catalysts [1], electrolytes [2] and other fuel cell components [3], and for the research on the influence of hydrogen fuel impurities [4,5], because they are easier to handle and consume less cell materials or fuel. However, the electric generation performance of a single cell itself is affected by its structure and component materials [6], as well as the driving method [7].

Regarding hydrogen fuel, a reliable hydrogen quality standard for fuel cell vehicles (FCV) should be established to accelerate the development of the hydrogen infrastructure and FCV technologies. To do this, reliable evaluation procedures including single cell hardware are needed to investigate the effect of impurities in hydrogen on fuel cell performance.

The Japan Automobile Research Institute (JARI) has been evaluating the influence of impurities on fuel cell performance by using JARI's standard single cell test procedure including single cell hardware, test equipment, test method, and evaluation method.

This paper reports on the cell hardware of JARI's standard single cell for the stable evaluation of fuel impurities, etc. [8,9].

2. Experimental

Fig. 1 schematically shows JARI's standard single cell. The configuration is similar to single cells used in laboratories for testing membrane and electrode assemblies ("MEAs"). The cell mainly consists of end plates (clamping plates), current collectors, and graphite flow-channel blocks. To determine the configuration, the effects of structure, materials, assembly method, and temperature control method on cell performance were investigated.

First, the frequency distribution of active electrode areas appearing in the literature was investigated to determine the active electrode area of JARI's standard single cell.

Second, the flow channel configuration of graphite blocks was determined by measuring the electric generation performance of MEAs of identical specifications with an electrode area of 25 cm^2. The MEAs were PRIMEA® 5510/5510 as-

* Corresponding author. Tel.: +81 29 856 0818; fax: +81 29 856 1169.
E-mail address: yhashi@jari.or.jp (Y. Hashimasa).

0378-7753/$ – see front matter © 2005 Elsevier B.V. All rights reserved.
doi:10.1016/j.jpowsour.2005.02.090

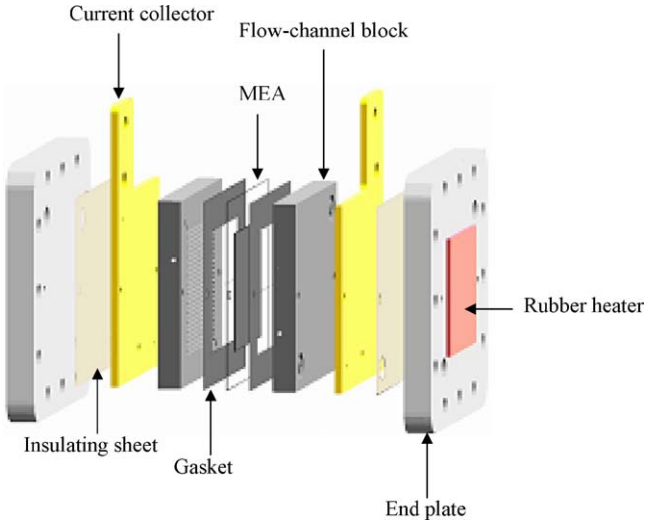

Fig. 1. Schematic of configuration of JARI's standard single cell.

semblies of Japan Goretex. Hydrogen with a dew point of 80 °C and air with a dew point of 60 °C were supplied at the hydrogen utilization ratio of 70% and air utilization ratio of 40%. The cell was operated at 80 °C, and at atmospheric backpressure.

Third, contact resistances between several carbon plates and TORAY™ carbon paper TGP-H060 were examined to select the material of flow-channel blocks and suitable contact pressure between flow-channel block and gas diffusion material when the cell is compressed.

Fourth, the effects of cell clamping torque on pressure distribution between flow-channel blocks and of gasket thickness on cell resistance were investigated to determine the method for assembling JARI's standard single cell.

Fifth, the effects of cell heating methods on cell temperature distribution were investigated to determine the temperature control method for JARI's standard single cell. To evaluate the electric generation performance, the cell must be heated to a prescribed temperature. Such temperature control is particularly important when examining the electrode catalyst's resistance to carbon monoxide poisoning [10], which is highly dependent on cell temperature. Three heating methods were tried: (1) constant temperature oven heating, (2) heater heating using a heating plate embedded with a cartridge heater or a rubber heater, and (3) heat medium heating using a water circulator. From the results, the final temperature control method for JARI's standard single cell was decided.

3. Results and discussion

3.1. Examination of cell configuration

3.1.1. Active electrode

The frequency distribution of the active electrode areas of single cells used at various research institutes reported in the literature was investigated (Fig. 2). It was found that active electrode areas of stack modules were larger than 100 cm^2, while active electrode areas of single cells and compact modules were less than 100 cm^2, and the frequency of 25 cm^2 was the highest. Therefore, an active electrode area of 25 cm^2 was selected for JARI's standard single cell.

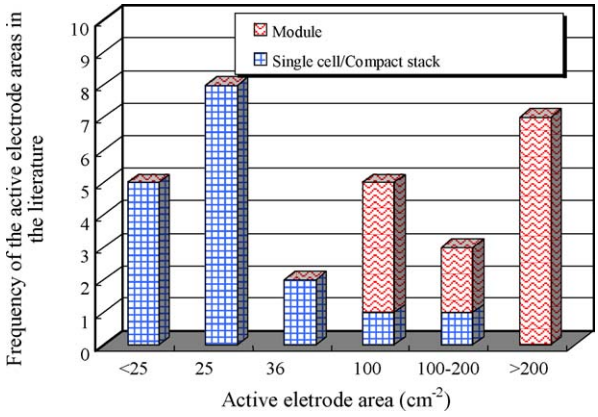

Fig. 2. Frequency distribution of active electrode areas used at various research institutes.

3.1.2. Examination of flow channel configuration

As the flow channel configuration in the cathode section is thought to have a large influence on power generation, the effect of the width of the flow channel in the cathode section was examined using JARI's standard single cell. The flow-channel block in the anode section was as shown in Table 1, while that in the cathode section had one flow channel with a channel interval of 1 mm and channel depth of 1 mm. Three different channel widths were tested. The current–voltage characteristics are given in Fig. 3, cell resistance in Fig. 4, and current–voltage (IR-free) characteristics in Fig. 5.

The voltage drop accelerated as the flow channel width increased (Fig. 3), possibly due to the increase of cell resistance resulting from the larger channel width (Fig. 4). Since a larger channel width reduces the contact area between the flow-channel block and gas diffusion material, the contact resistance is increased. Even though the voltage drop caused by the cell resistance factor was eliminated, an increase in the flow channel width resulted in the acceleration of voltage drop (Fig. 5). This was attributed to an increase in gas distribution polarization resulting from the slower gas flow inside the widened channel.

Table 1
Configuration of flow channel used for JARI's standard single cell

Outer diameter; thickness	80 mm^2; 10 mm thick
Configuration of electrode (active electrode area)	50 mm × 50 mm (25 cm^2)
Number of flow channels; configuration	One; serpentine
Flow channel width	1 mm
Flow channel interval	1 mm
Flow channel depth	1 mm

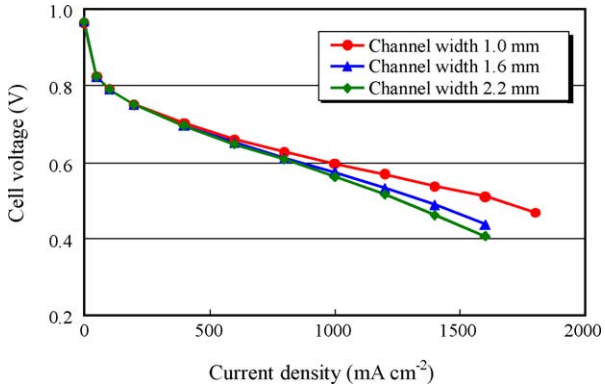

Fig. 3. Effect of flow channel width on cell voltage.

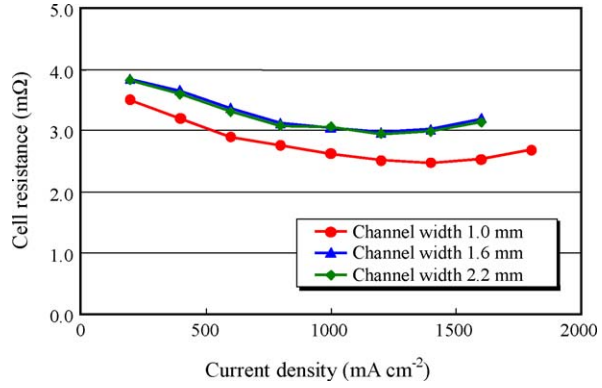

Fig. 4. Effect of flow channel width on cell resistance.

The cathode section flow-channel block had one flow channel of 1 mm width and 1 mm between channels, and three different channel depths were tested. The resulting current–voltage characteristics are shown in Fig. 6, and cell resistance in Fig. 7. Even though the voltage drop accelerated as the flow channel depth increased (Fig. 6), the flow channel depth did not influence the cell resistance (Fig. 7). Since channel depth has no influence on the contact area between the flow-channel block and gas diffusion material, it would not affect the contact resistance. It was confirmed that

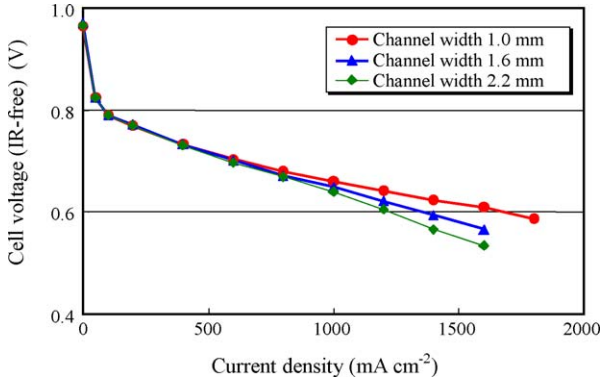

Fig. 5. Effect of flow channel width on cell voltage (IR-Free).

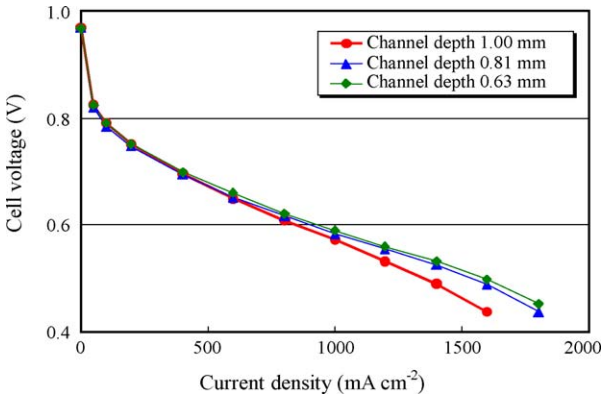

Fig. 6. Effect of flow channel depth on cell voltage.

the cell performance could be enhanced by reducing the flow channel depth and preventing the voltage drop caused by the decrease in gas distribution polarization resulting from the larger gas flow rate. However, if the channel depth is too shallow, the pressure drop in the flow channel increases. A channel depth of 1 mm is sufficient to achieve stable cell performance for estimating the effects of impurities. Similar tests were conducted to determine the influences of flow channel interval and configuration, which were then decided as shown in Table 1.

3.2. Examination of flow-channel block materials

To select the flow-channel block material, the contact resistances between several materials for flow-channel block and carbon paper were measured by the four-probe method of resistivity measurement. The effect of the applied load on the contact resistance is shown in Fig. 8 The contact resistance of resin-impregnated high-density artificial graphite was the least irrespective of the applied load, and it became small and stable when the contact pressure exceeded 10 kgf cm^{-2}. Therefore, we chose this material for the flow-channel block, and the target contact pressure when the cell was compressed by applying a torque on each bolt was set as 10 kgf cm^{-2}.

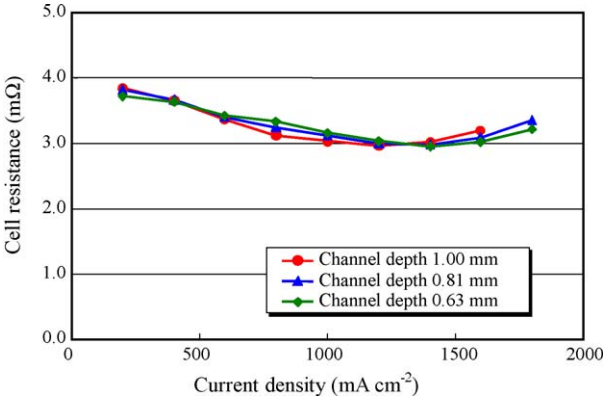

Fig. 7. Effect of channel depth on cell resistance.

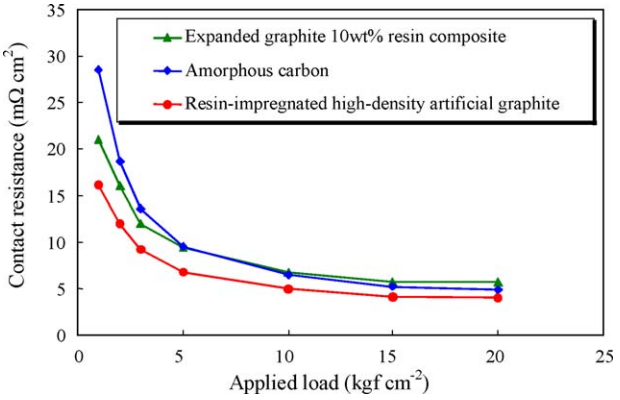

Fig. 8. Effect of separator materials on contact resistance.

3.3. Examination of cell assembly method

3.3.1. Clamping torque

The effect of clamping torque was investigated to decide the cell assembly method. The relationship between tightening force and clamping torque is:

$$N \times T = K \times d \times P \quad (1)$$

where N is the number of bolts, T the clamping torque, K the torque constant, d the nominal bolt diameter, and P is the tightening force.

From the result of Section 3.2, tightening force P must be more than 10 kgf cm^{-2}.

The relationship between the tightening force and the deflection of the rectangular plate is:

$$W = \frac{\alpha \times P \times a^4}{t^3 \times E} \quad (2)$$

where W is the deflection of rectangular plate, α the bending coefficient, P the tightening force, a the length of plate, t the thickness of plate, and E is the elastic coefficient.

In this equation, the deflection of the rectangular plate W should be zero for good contact between cell components.

From these equations, the number of bolts, clamping torque, and thickness of clamping plate were set as 12, 40 kgf cm, and 12 mm, respectively. Under these conditions, the contact pressure distribution between anode and cathode flow-channel blocks was measured by pressure-sensitive sheets that change color according to the compressed pressure when the cell was compressed by applying a torque on each bolt. Fig. 9 shows the contact pressure distribution between flow-channel blocks measured by Prescale (Fujifilm). It was found that the contact pressure distribution was very even. The number of bolts, clamping torque, and thickness of clamping plate were selected as 12, 40 kgf cm, and 12 mm, respectively.

3.3.2. Gasket thickness

The effect of the gasket thickness used in the cell assembly was investigated. Fig. 10 shows the change in cell resistance

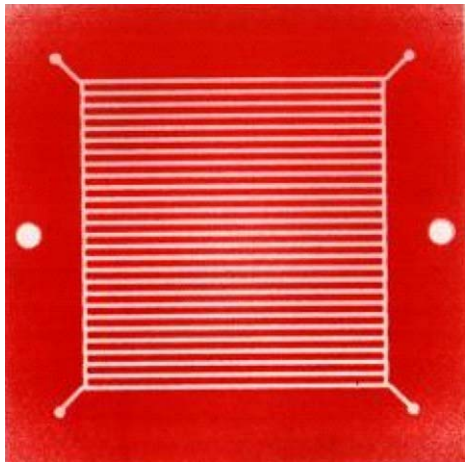

Fig. 9. Distribution of contact pressure between flow-channel blocks of JARI's standard single cell.

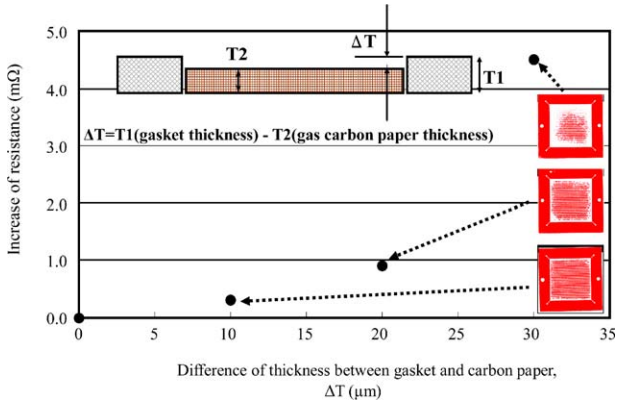

Fig. 10. Effect of the thickness difference between gasket and carbon paper on cell resistance.

in relation to gasket thickness when assembling the cell using the same carbon paper thickness and clamping torque of 40 kgf cm and by changing the thickness of the gasket of the same material. The electrical resistance was measured by an LCZ meter at the frequency of 1 kHz. In the figure, the color changes for each gasket thickness are shown. Here, ΔT is the difference in thickness between the gasket and carbon paper: $\Delta T = T_1$ (gasket thickness) $- T_2$ (carbon paper thickness). As ΔT increased, the cell resistance increased exponentially. Note that the cell resistance became small and stable when ΔT was within 10 μm because of good contact between the carbon paper and graphite flow-channel block. The gaskets should preferably be of the same thickness as the carbon paper; for JARI's standard single cell, gaskets of the same thickness to within 10 μm are used for all units and tests.

3.4. Examination of cell temperature control methods

3.4.1. Cell composition and temperature measurement positions

The temperature distribution of JARI's standard single cell during electric generation was investigated, for the cell com-

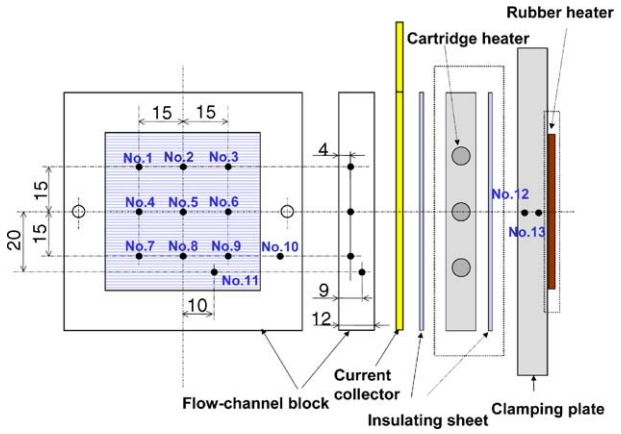

Fig. 11. Temperature measurement position.

position and temperature measurement positions (No. 1–13) shown in Fig. 11. Both the rubber heater method and cartridge heater method are shown in this figure. A common clamping plate, current collector and graphite flow-channel block were used in all heating methods. In the rubber heater method, a rubber heater of 50 mm × 50 mm was attached to the outside of the clamping plate. In the cartridge heater method, a heating plate was embedded with one or three cartridge heaters and was interposed between the current collector and the clamping plate. In all methods, cell temperature was measured during electric generation at positions No. 1–13 in Fig. 10 by a thermocouple. The ungrounded type of measuring junction was used because it is not restricted by the object to be measured and the element is covered with an insulator. Positions No. 1–9 and 11 were in the reaction area of the graphite flow-channel block, No. 10 was outside of the reaction area, and No. 12 and 13 were in the clamping plate. The cell temperature was controlled so that the temperature at position No. 11 was maintained at 80 °C. Hydrogen with a dew point of 80 °C and air with a dew point of 70 °C were supplied at flow rates of 435 and 1630 mL min^{-1}. The cell was operated under continuously increasing load. The duration at each current density was a constant 3 min. Fig. 12

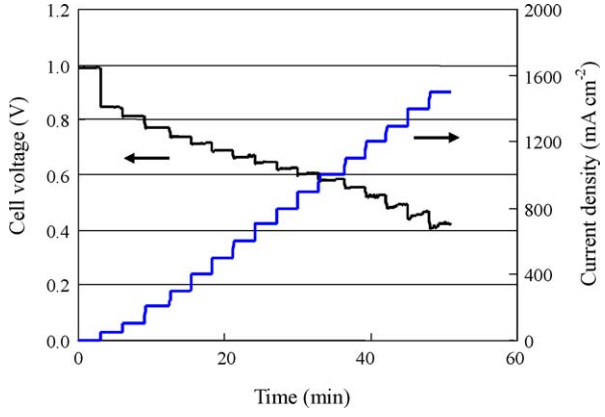

Fig. 12. Cell voltage response under continuously increasing load.

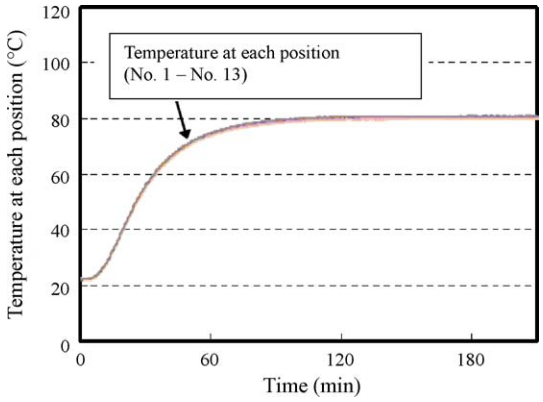

Fig. 13. Changes in temperature at each position by constant oven heating without electric generation.

shows the relationship between current density and operating time in this experiment. The increase of time means the increase of current density during electric generation in later figures.

3.4.2. Constant temperature oven heating

The single cell without rubber heater or heating plate was placed inside the constant temperature oven at room temperature, and heating was carried out with the oven set to 80 °C. The changes in temperature at each position of the cell are shown in Fig. 13. It took about 90 min for the single cell to reach the set temperature. However, the maximum temperature difference inside the cell was very small and the temperature distribution was even.

Next, cell temperature was measured during electric generation. Fig. 14 shows the changes in temperature at each position of the cell during electric generation. The cell temperature rose as the current density increased and the temperature in the graphite flow-channel block was higher than that of the clamping plate. The temperature at position No. 13 in the clamping plate was lower than that at position No. 12. In the case of constant temperature oven heating, the ambient temperature was set to a constant 80 °C, so the amount radiating to the outside was small in relation to the calorific

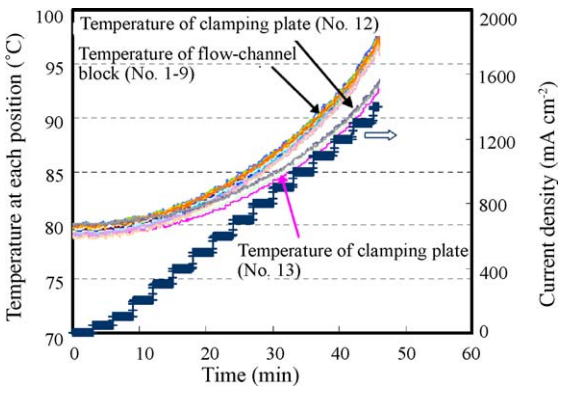

Fig. 14. Changes in temperature at each position by constant oven heating during electric generation.

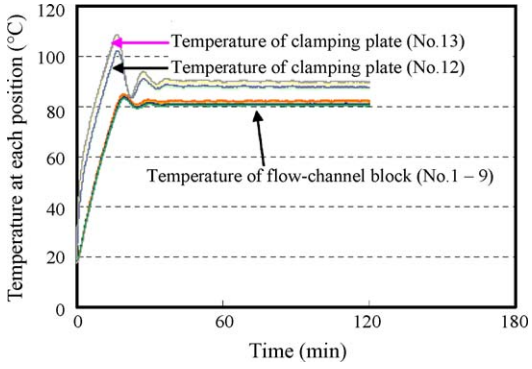

Fig. 15. Changes in temperature at each position by rubber heater heating without electric generation.

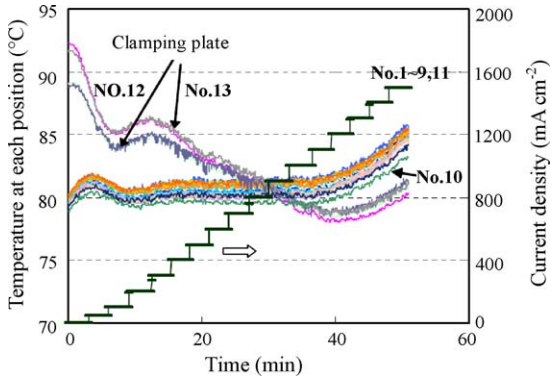

Fig. 16. Changes in temperature at each position by rubber heater heating during electric generation.

power because of electric generation, thus leading to the rise in temperature of the cell. It would be difficult to control cell temperature only by this heating method even if the ambient temperature were to be controlled.

3.4.3. Heating by heater

Temperature control was performed by means of a rubber heater attached to the outside of the clamping plate at both electrodes. The change in temperature when the single cell was heated from room temperature to 80 °C by PID (P, proportional; I, integral; D, derivative) control is shown in Fig. 15. PID control involves approaching the target value by simultaneously performing proportional action (P action), which produces an output in proportion to the deviation of the present value (PV) from the set value (SV); integral action (I action), which produces an output in proportion to the integral of the deviation; derivative action (D action), which produces an output in proportion to the derivative of the deviation. This figure shows that the temperature at position No. 13 in the clamping plate on the heater side was higher than the temperature at No. 12 in the clamping plate on the flow-channel block side, because the cell was heated by the rubber heater attached to the outside of the clamping plate. However, temperatures at each position from Nos. 1–9 in the reaction area of the flow-channel block rose to 80 °C and the temperature distribution in the reaction area was very small.

Next, the current–voltage characteristics were measured under this condition. The temperature variations in the various parts of the cell heated by a rubber heater are shown in Fig. 16. In the clamping plate, the temperature at position No. 13 was higher than that at position No. 12 in the low current density region because the cell was heated by the rubber heater attached to the outside of the clamping plate, and the temperature at position No. 12 was higher than that at position No. 13 in the high current density region because of the generated heat. Regarding the graphite flow-channel block, the temperatures at each position from Nos. 1–9 in the reaction area of the flow-channel block were even at 80 °C, and the temperature at position No. 10 outside the reaction area was always lower than that inside the reaction area (positions No. 1–9 and 11). To regulate the cell temperature precisely, the temperature for control should be measured in the reaction area of the graphite flow-channel block because the temperature in the reaction area of the flow-channel block differs from that outside the reaction area or the temperature in the clamping plate. Therefore, the center of the reaction area of the graphite flow-channel block was selected as the point of temperature control for JARI's standard single cell.

Next, the temperature difference between with rubber heater heating and with cartridge heater heating was investigated. The maximum temperature difference among the 9 positions in the reaction area (total 18 positions for both anode and cathode sections) is shown in Fig. 17. The maximum temperature difference was smaller with a rubber heater than with cartridge heaters, indicating a more uniform heat distribution by the rubber heater.

3.4.4. Heat medium heating

Temperature control was performed by a water circulator equipped with a heater and a refrigerating machine. The cell temperature was controlled so that the temperature at position No. 11 was maintained at 80 °C by PID control. Two types of cell were prepared for the test as shown in Fig. 18. In the type A cell, the water path in the clamping plate was outside the

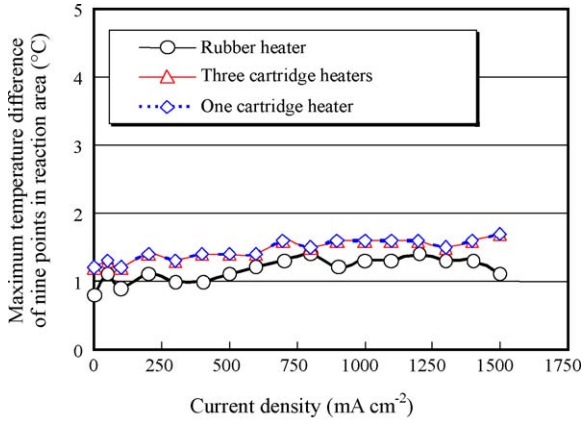

Fig. 17. Relationship between maximum temperature difference of nine points in reaction area and current density.

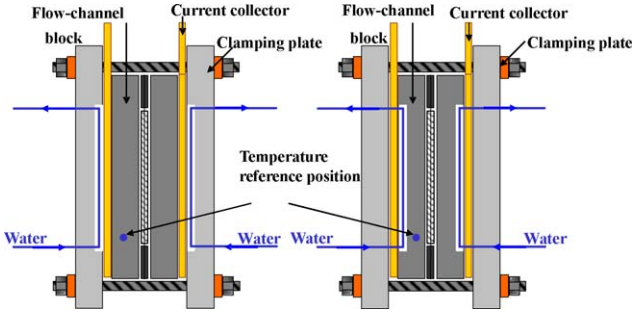

Fig. 18. Schematic image of cooling path in cells.

insulating sheet and current collector. In the type B cell, the water path in the graphite flow-channel block was inside the insulating sheet and current collector. The area of the flow channel for the heat medium was set to 50 mm × 50 mm, the same as the area of the electrode.

The temperature variations in the various parts of cells heated by the heat medium without electric generation are shown in Fig. 19. Whereas the type A cell could not control cell temperature stably, the type B cell could do so. This is probably because heat was not transferred smoothly in the type A cell due to the presence of the insulating sheet and current collector between the water and the temperature reference position for control. Thermal conductivity between the graphite flow-channel block (temperature reference position) and water path might influence the stability of cell temperature.

The effects of heating method (rubber heater heating and heat medium heating) on the relationship between average temperature of the nine positions (Nos. 1–9) in the reaction area and current density were as shown in Fig. 20. It was found that, when heated by the heat medium, the average temperature in the reaction area was stable throughout the current density region, and that when heated by a rubber heater, the average temperature in the reaction area rose in the high current density region. This was because the amount of generated

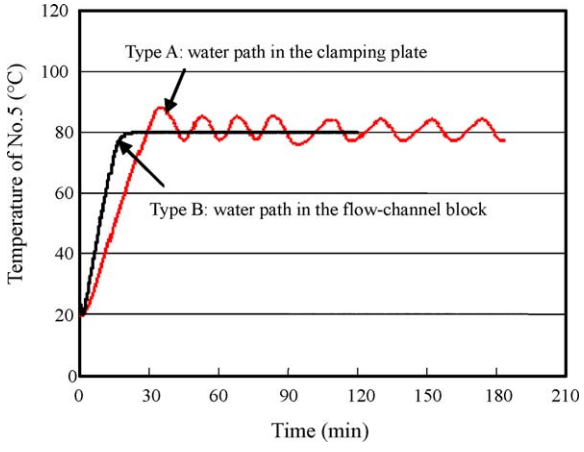

Fig. 19. Changes in temperature at each position by heat medium heating without electric generation.

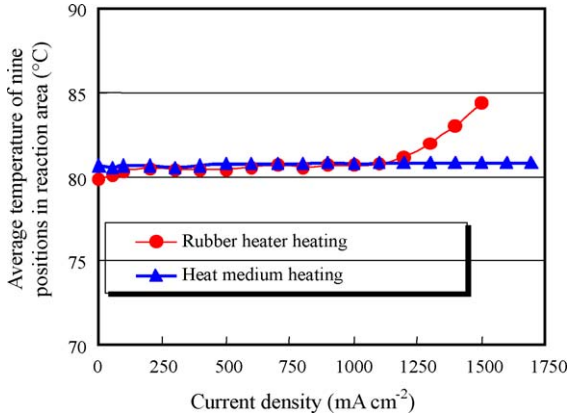

Fig. 20. Effect of heating method on the relationship between average temperature of nine positions in reaction area and current density.

heat rises in the high current density region, exceeding the cell's heat radiation capacity. Heat medium heating can control cell temperature stably, but the facility becomes complicated. Rubber heater heating can control the cell temperature stably up to 1200 mA cm^{-2}, and is easy to handle. Therefore, rubber heater heating was selected for JARI's standard single cell for estimating fuel impurities conducted at mainly 1000 mA cm^{-2}. To estimate the maximum output power or the performance of gas diffusion materials, another heating method must be used to achieve temperature stability in the region of higher current density.

3.5. *Electric generation performance of JARI's standard single cell*

Finally, the reproducibility from one test to another was investigated. Electric generation was evaluated by applying MEAs of identical specifications and test conditions. Hydrogen with a dew point of 80 °C and air with a dew point of 60 °C were supplied at the hydrogen utilization ratio of 70% and air utilization ratio of 40%. The cell was operated at 80 °C, and at atmospheric backpressure. The cell was operated under continuously increasing load. The duration at each current

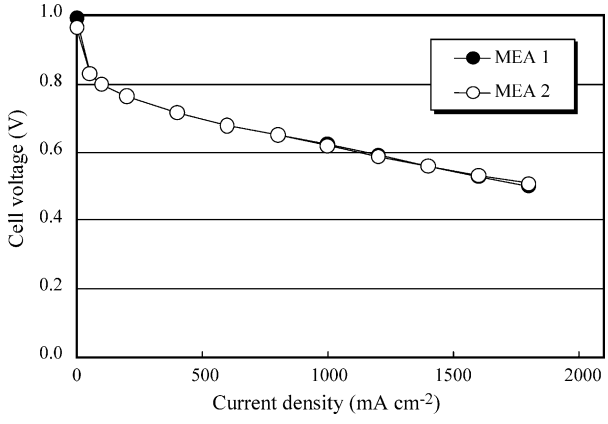

Fig. 21. Current–voltage characteristics of JARI's standard single cell.

density was a constant 3 min. The results for current–voltage characteristics are given in Fig. 21. This figure reveals that the performance reproducibility of two MEAs is excellent, and that stable evaluations could be performed by JARI's standard single cell.

4. Conclusion

This study was conducted to develop JARI's standard single cell for investigating the influence of impurities in hydrogen fuel. Cells having different structures yielded different results, even though their MEAs were identical. From the measured effects of the flow channel configuration of flow-channel block and the cell assembly method, and the cell's heating method, a suitable flow-channel configuration, cell assembly procedures, and thermal design were determined. Because these cells are easily assembled and disassembled, generate electricity uniformly from one unit to another, and have high reproducibility from one test to another, they are widely used by JARI and other laboratories alike.

Acknowledgements

This paper is part of the project for establishing codes and standards for PEFC vehicles, which is in progress by the Japan Automobile Research Institute under a contract with the New Energy and Industrial Technology Development Organization (NEDO).

References

[1] A.T. Haug, R.E. White, J.W. Weidner, W. Huang, S. Shi, T. Stoner, N. Rana, J. Electrochem. Soc. 149 (3) (2002) A280–A287.
[2] J.A. Asensio, S. Borros, P. Gomez-Romero, J. Electrochem. Soc. 151 (2) (2004) A304–A310.
[3] K. Scott, W.M. Taama, P. Argyropoulos, J. Appl. Electrochem. 28 (1998) 1389–1397.
[4] B. Rohland, V. Plzak, J. Power Sources 84 (1999) 183–186.
[5] K.A. Starz, E. Auer, Th. Lehmann, R. Zuber, J. Power Sources 84 (1999) 167–172.
[6] W.-K. Lee, C.-H. Ho, J.W. van Zee, M. Murthy, J. Power Sources 84 (1999) 45–51.
[7] K.T. Adjemian, S.J. Lee, S. Srinivasan, J. Benziger, A.B. Bocarsly, J. Electrochem. Soc. 149 (3) (2002) A256–A261.
[8] Y. Hashimasa, et al., Development of JARI standard single cell for testing cell materials (1), JARI Res. J. 24 (10) (2002) 41–44.
[9] Y. Hashimasa, et al., Development of JARI standard single cell for testing cell materials—effect of cell heating method on cell temperature distribution, JARI Res. J. 25 (12) (2003) 25–28.
[10] H. Fukumoto, et al., Study of CO poisoning in PEFC anode and catalysts for CO resistance, in: Proceedings of the Fifth FCDIC Fuel Cell Symposium, June 1998, pp. 112–115.